Archives of Hydro-Engineering and Environmental Mechanics
Vol. 49 (2002), No. 1, pp. 3–21

Simulation of Three-dimension Side Discharge into an Open Channel

Yafei Jia*, Włodzimierz Czernuszenko[1], Sam S. Y. Wang***

* National Center for Computational Hydroscience and Engineering, The University of Mississippi, University, MS 38677, USA. E-mail: jia@ncche.olemiss.edu

** Polish Academy of Sciences, Institute of Geophysics, 01–452 Warsaw, Ks. Janusza 64, Poland. E-mail: wczer@igf.edu.pl

(Received July 4, 2001; revised January 15, 2002)

Abstract

A three-dimensional computational model, solving Reynolds equations with the k-ε turbulence closure, has been presented to simulate the flow field in an open channel near a side-discharge channel. The purpose of this study was to exam this model's applicability for simulating the three-dimensional recirculation velocity field in the vicinity of the side discharge channel. The numerical simulations show that both the height and length of the recirculation zone were correctly predicted when compared with laboratory measurements. The predicted trend of the shape of the recirculation zone under different flow conditions agrees with experimental data. It was confirmed that the SMART upwinding scheme performs better than QUICK and HYBRID schemes, since it induces less numerical diffusion and no oscillations. It was found in this study that the SMART scheme needs some minor modifications for complex flow computations.

Notation

b – width of discharge channel,
B – width of main channel,
E – roughness parameter,
g – gravitational acceleration,
h – local water depth,
h_o – mean water depth,
H – lateral size of the recirculation eddy,
k – turbulence energy,
L – longitudinal size of the recirculation eddy,

[1] Corresponding author.

p – pressure,
p_* – pressure,
R_m – momentum flux ratio,
U_o – mean velocity in the main channel,
V_d – mean velocity in the discharge channel,
u, v, w – time-averaged velocity components in x, y, and z directions, respectively.
u', v', w' – turbulence intensity in x, y, and z directions, respectively.
u_* – shear velocity,
ε – turbulence energy dissipation rate,
Γ_n – numerical diffusivity,
ρ – density of water,
η – water surface elevation,
ν, ν_t – kinematic and turbulence eddy viscosity
τ – shear stress.

Subscripts

i, j – positive integer indices,
d – discharge channel,
o – main channel.

1. Introduction

The discharge of waste water into rivers causes ecologically degraded zones with relatively high pollutant concentration stretching far downstream. High velocity of the side discharge would sometimes result in erosion and deposition in the area of recirculation developed by turbulent jet and river flow. Pollutant concentration trapped in the recirculation zone would be much higher than that in the far field area and could cause serious ecological problems in the near field area. Predicting the flow configuration and concentration distribution in the polluted zones is one of the major problems in environmental engineering nowadays.

Interaction of the main flow and side discharge has been an interesting research topic for many researchers. Strazisar and Prahl (1973) performed physical experiments on turbulent jet entering perpendicularly into the channel flow. Based on the measured trajectories of the jet and sizes of the recirculation zone, it was found that the longitudinal sizes of a recirculation zone depend on the ratio of jet to channel velocities and widths, but not on the flow depth. An equation for calculating the trajectory of the jet was developed. Mikhail et al. (1975) conducted similar physical experiments and concluded that the transversal height of the

recirculation zone in wide channels depends only on the ratio of momentum flux of the jet and the channel flow. They pointed out that the ratio of the longitudinal and transversal sizes of a recirculation zone is almost constant and does not depend on the flux ratio.

As physical experiments are expensive and data available not as much as one desires, numerical modelling has been conducted to examine the performance of numerical schemes and explore the applicability of numerical models to simulate complex flows. McGuirk and Rodi (19780 considered the perpendicular side discharge of the passive pollutants into the wide open channel over the total water depth. They proposed a 2D mathematical model to calculate the depth averaged velocity field in the vicinity of the discharge. The model, however, cannot account for 3D features of side discharge. Rodi and Srivatsa (1980) proposed a 3D finite difference calculation procedure for a small reverse-flow region. The procedure treats the reverse-flow region as elliptic only and the rest of the flow as either parabolic or partially parabolic. The hybrid difference scheme was used to solve the governing differential equations. They concluded that the procedure gives much better results than the parabolic, as well as the partially-parabolic approach.

Recognizing the importance of the estimation of the convective/advective terms to the success of simulating hydrodynamics and transport, upwinding techniques were studied and evaluated using general transport problems and the side discharge case. Leschziner (1980) considered the steady state, laminar plane and axially symmetric recirculating flows. When solving partial differential equations, three finite difference discretizations were used, namely: hybrid central/upwind, hybrid central/skew-upwind and QUICK scheme developed by Leonard (1979). Applications of these schemes to laminar, recirculating flows have shown that strong artificial diffusion was introduced by the first scheme and boundedness problems by others. Demuren (1983) presented the results of the numerical calculation of the steady 3D turbulent jets in a cross-flow. Turbulence effects were modelled by the k-ε model. The basic equations were solved using two finite-difference numerical procedures, the quadratic upstream weighted (QUICK) and the hybrid/upwind difference scheme. The results depend on the numerical scheme and the widely employed hybrid scheme introduced a serious error, which was interpreted as false or numerical diffusion.

Demuren and Rodi (1983) applied a 3D mathematical model to describe the velocity field in an open channel flow just below the outlet of perpendicular side discharges. They employed the time-averaged equations governing the mass and momentum conservation for the turbulent flow in an open channel together with k-ε turbulence model. Using both the hybrid central/upwind differencing approach and the QUICK scheme solved the equations. The numerical predictions of the size of the recirculation zone were compared with measurements for smooth and rough bed channels. The QUICK scheme predicted the length of the recirculation zone correctly in both the smooth-bed and rough-bed cases. The Hybrid scheme

underestimated the size of the recirculation zone as much as 50% due to numerical diffusion. Estimated numerical diffusion coefficient for a 2D case indicated that the ratio of numerical to physical diffusivity could be as much as 50.

Although its accuracy is high, the weakness of the QUICK scheme is the numerical oscillation where high concentration gradient is concerned. Gaskell and Lau (1988) pointed out the importance of numerical boundedness to accuracy and stability. A new numerical algorithm SMART, which preserves a boundedness and maintains a high degree of accuracy, was derived. Leonard and Niknafs (1991) adopted a similar concept of numerical boundedness and came up with a high order, non-oscillatory upwinding scheme: ULTIMATE.

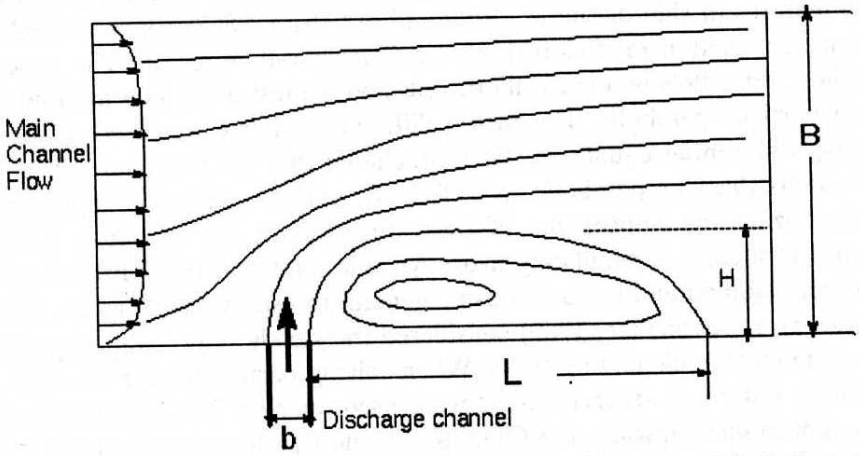

Fig. 1. Sketch of the flow pattern ($x - y$ plane), channel configuration and basic dimensions

The present paper considers a simplified problem: water is discharged perpendicularly into a straight river channel. A 3D turbulent jet is formed and bends over by the river flow. On the other hand the river flow is diverted by the side discharge towards to the bank opposite to the side discharge entrance. Interaction of the jet and the channel flow leads to the formation of a very complex flow field – the recirculation zone behind the jet near the bank (Fig. 1). The 3D mathematical model for simulating the flows in the vicinity of the side discharge is presented. The model is based on Reynolds equations governing a steady, uniform-density flow. The turbulence stress terms, representing the transport and mixing of momentum by the turbulent fluctuations, are expressed by eddy-viscosity concept and k-ε closure. This model can be used to predict the flow field and recirculation configuration, in particular, the sizes of the recirculation eddy, location of the reattachment point and the magnitude and direction of velocity at any point within the recirculation eddy. Results from both experimental and theoretical approaches were used to examine the shape of recirculation zones.

2. Mathematical Model

Three-dimensional open channel flows can be described by the mass and momentum conservation laws. The turbulence stresses are related to the mean rate of strains and the eddy viscosity according to Boussinesq's assumption. These basic equations can be written in the form:

$$\frac{\partial u_j}{\partial x_j} = 0, \tag{1}$$

$$\frac{\partial u_j u_i}{\partial x_j} - \frac{\partial}{\partial x_j}\left[(\nu_t + \nu)\left(\frac{\partial u_j}{\partial x_i} + \frac{\partial u_i}{\partial x_j}\right)\right] + \frac{1}{\rho}\frac{\partial p_*}{\partial x_i} = 0, \tag{2}$$

$$p_* = p + \rho g z, \tag{3}$$

where subscripts i and j may vary from 1 to 3, and stand for longitudinal, transvers and vertical components of the Reynolds averaged velocity in x, y, and z directions, respectively. Notations, u, v, and w for velocities in these three directions will also be used, ν_t is turbulent eddy viscosity and ν is kinematic viscosity, p_* is the piezometric pressure, solved in the same way as that used by Long, Steffler, and Rajaratnam (1991), and p is total pressure. Eddy viscosity was modeled by the equation:

$$\nu_t = C_\mu \frac{k^2}{\varepsilon}. \tag{4}$$

The transport equations were solved for turbulence kinetic energy k, and energy dissipation rate ε:

$$\frac{\partial k u_j}{\partial x_j} - \frac{\partial}{\partial x_j}\left(\frac{\nu_t}{\sigma_k}\frac{\partial k}{\partial x_j}\right) = P + \varepsilon, \tag{5}$$

$$\frac{\partial \varepsilon u_j}{\partial x_j} - \frac{\partial}{\partial x_j}\left(\frac{\nu_t}{\sigma_\varepsilon}\frac{\partial \varepsilon}{\partial x_j}\right) = C_1\frac{P\varepsilon}{k} - C_2\frac{\varepsilon^2}{k}, \tag{6}$$

$$P = \nu_t\left(\frac{\partial u_i}{\partial x_j} + \frac{\partial u_j}{\partial x_i}\right)\frac{\partial u_i}{\partial x_j}. \tag{7}$$

Standard coefficients were adopted, i.e., $C_\mu = 0.09$, $C_1 = 1.44$, $C_2 = 1.92$, $\sigma_k = 1.0$, $\sigma_\varepsilon = 1.3$.

3. Boundary Conditions

To solve these governing equations, boundary conditions must be prescribed at all boundaries: the inlet, outlet, solid walls and water surface. The boundary conditions at the inlet section are particularly important for the turbulence transport equations. Realistic solutions would depend on proper evaluations of the kinetic

energy and the energy dissipation rate at this section. There are a several approaches to estimate boundary values for the k-ε model. Rastogi and Rodi (1980) used an uniform distribution in the inlet section by applying depth-averaged values of k and ε. Leschziner (1980) specified the inlet boundary conditions for k using experimental data and for ε using equation $\varepsilon = C_\mu^{3/4} k^{3/2} L_m$, L_m is a mixing length.

In this study, the semi-empirical relationships for the turbulence intensities (Nezu and Rodi 1986) were adopted for the estimation of the kinetic energy at the inlet cross-section, assuming that flow was fully developed.

$$\frac{u'}{u_*} = D_u \exp(-\lambda_u \xi)\Gamma + 0.3 z^+ (1 - \Gamma), \tag{8}$$

$$\frac{w'}{u_*} = D_w \exp(-\lambda_w \xi), \tag{9}$$

$$\Gamma = 1 - \exp\left(-\frac{z^+}{B'}\right), \tag{10}$$

where u' and w' are turbulence intensities in longitudinal and vertical directions, respectively. u_* is shear velocity of the main flow at the entrance, $\xi = z/h$, D_u=2.26, D_w=1.23, λ_u =0.88, λ_w=0.67, B'=10, $z^+ = zu_*/v$, Γ is the van Driest damping function, and h is the local water depth. Together with the assumption that the turbulence intensity in the transvers direction is equal to that in the vertical direction and the definition:

$$k = \frac{u'^2 + v'^2 + w'^2}{2}, \tag{11}$$

one can obtain the boundary values of kinetic energy at the inlet cross-section. Although these relationships were obtained in the central plane of the channel, they applied to the whole cross-section. Errors introduced were considered negligible, since the channel flows studied in the paper were of shallow water, and the inlet section was placed some distance from the discharge channel. Turbulence eddy viscosity at the inlet cross-section was assumed parabolically distributed as suggested by experimental data and analytical considerations (Nazu and Rodi 1986).

$$\nu_t = \kappa u_* h (1 - \xi)\xi, \tag{12}$$

where $\kappa = 0.41$ is the Karman constant. The turbulence energy dissipation rate ε was obtained from equation (4). This approach has been used to produce reasonable results of channel flow simulations [6]. The inlet section was located at $x = 14h_0$ (h_0 is the mean water depth) upstream of the discharge outlet. A transversal distribution of flow discharge per unit width was specified as a power function of distance from the wall with a power of 1/7, and the vertical distribution of velocities of the inlet section was assumed to be logarithmic. Variables thus specified are shown in Fig. 2.

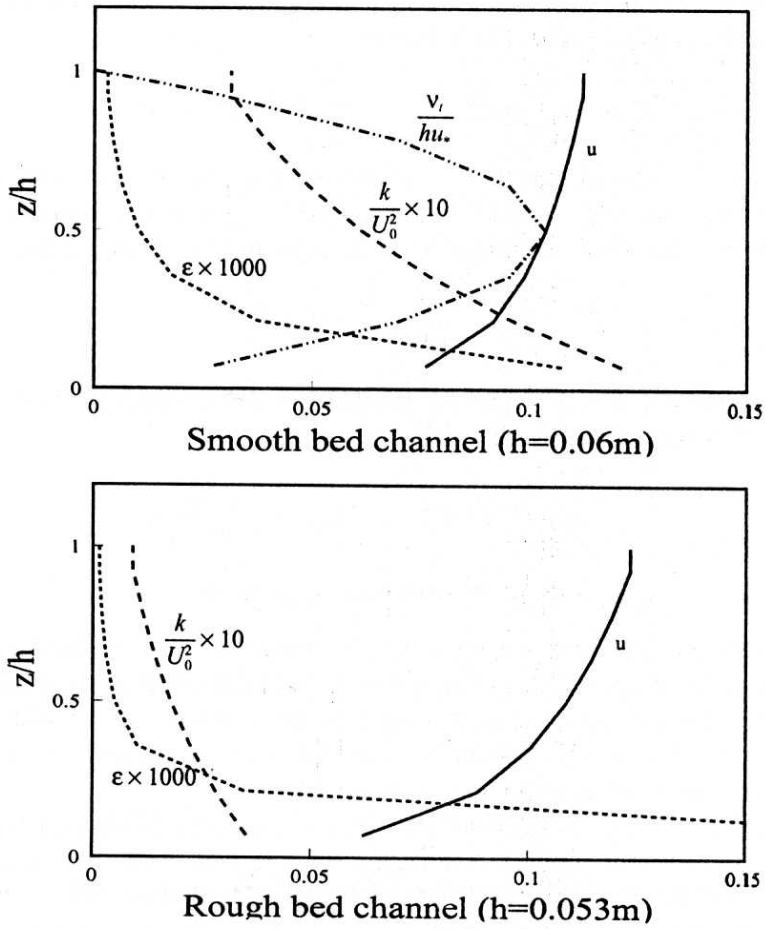

Fig. 2. Inlet boundary conditions velocity u (m/s), turbulence kinetic energy k (m^2/s^3), energy dissipation rate ε (m^2/s^3) and eddy viscosity ν_t (m^2/s)

At the outlet cross-section, longitudinal gradient of the variables u, v, w, p_*, k, and ε, were set at zero. At the water surface, the gradients of u, v, p^*, k and ε in the vertical direction were zero. The vertical velocity component at the water surface, can be obtained using the kinematics condition

$$w_\eta - u_\eta \frac{\partial \eta}{\partial x} - v_\eta \frac{\partial \eta}{\partial y} = 0, \tag{13}$$

where η is the water surface elevation and $p_* = \rho g \eta$ was applied at the water surface. The water surface elevation can be adjusted by $\partial p_*/\partial z$ near the surface (Rastogi and Rodi 1980). The numerical grid in the vertical direction was not adjusted due to water surface change as the variation of the surface was very small in this case. The logarithmic law of the wall was applied to compute shear

stress, and turbulence properties k and ε in regions very close to the channel bed as well as the vertical walls. The equation

$$u^+ = \frac{1}{\kappa}\ln(Ez^+), \qquad \text{for } 30 < z^+ < 300, \tag{14}$$

($u^+ = u/u_*$, $z^+ = zu_*/v$ and E is a roughness parameter) was solved iteratively to obtain shear velocity u_* and shear stress $\tau = \rho u_*^2$. The wall boundary values of k and ε were estimated assuming the local equilibrium of turbulence energy:

$$k = \frac{u_*^2}{C_\mu^{0.5}}, \qquad \varepsilon = \frac{u_*^3}{\kappa z}. \tag{15}$$

At the discharge channel, boundary values for k and ε were specified in the same way as in (Demuren and Rodi 1983), i.e.

$$k_d = 0.004V_d^2, \qquad \varepsilon_d = C_\mu^{3/4}\frac{k_d^{1.5}}{0.09b}. \tag{16}$$

4. Numerical Approach

Governing equations were solved using the control volume method and SIMPLE procedure (Patankar 1980). Staggered grid and ADI method were adopted. It is well known that a convection term is the most difficult to deal with when the flow is of convection dominance. Efforts have been made to approximate the convective phenomena more adequately and accurately.

Gaskell and Lau (1988) have developed a scheme (SMART) based on the concept of convective boundedness. The scheme was used to compute the first derivative of an unsteady, linear transport equation without source terms. As is well known, the interpolation method for evaluating the transported scalar at the control volume surface is the key to the success of the scheme. This scheme is stable according to Leonard's convective stability criteria (Leonard 1979), and accurate, and attractive as shown in (Falconer 1992). The SMART scheme virtually combines the scheme of QUICK and concept of a convective boundedness. It uses unwinding when variation of the concentration being transported is large and the interpolated value at the control volume surface is not bounded. The QUICK scheme is applied for cases in which the variation is mild and interpolation bounded. As a result, the SMART scheme avoids oscillating the nature of QUICK when concentration gradient is large and preserves a high order of accuracy for moderate variation of concentration. A similar idea was proposed in (Leonard and Niknafs 1991), where the convective boundedness was interpreted and formulated as the ULTIMATE limiter. The interpolation at the control volume surface by any method would satisfy the limiter and not be changed if monotonic, the interpolated value would be replaced by the nearest one in the limiter if this it is non-monotonic.

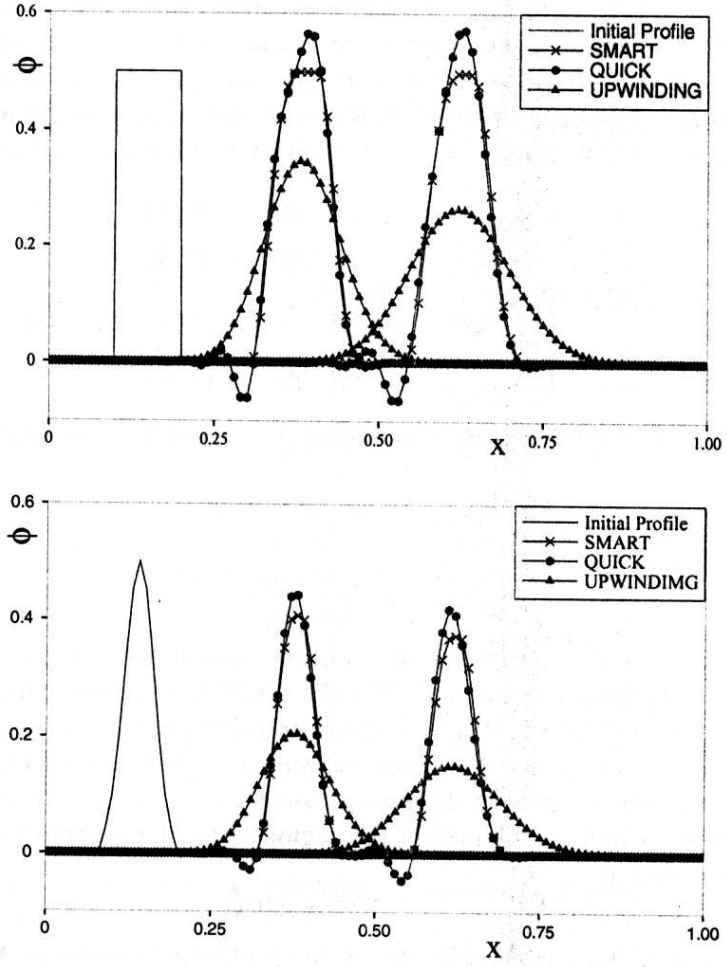

Fig. 3. Comparison of QUICK, UPWINDING and SMART scheme, ϕ – non-dimensional concentration, X – non-dimensional distance; figure above: transport of a concentration block, figure below: transport of a Gaussian Cone

Additional tests of a concentration block and Gaussian cone transport cases (Fig. 3) confirmed the conclusions: SMART is good in handling shock wave fronts, it induces no oscillations and negative concentration problems. However, it smooths the Gaussian cone faster than QUICK. The first order upwinding scheme showed unacceptable numerical diffusion in both cases. These comparisons confirmed the superiority of SMART, which was therefore adapted to SIMPLE procedure to compute the advection terms.

To demonstrate the SMART scheme, one can consider the transport in one dimensional space with uniform grid ($i-2$, $i-1$, i, $i+1$, ...). The centre of

the control volume is located at i, and the values at control volume surfaces: $i-1/2$ and $i+1/2$ are to be estimated. For velocity $u(i-1/2)>0$, the value of ϕ at $i-1/2$ is computed based on those located at $i-2$, $i-1$, and i. Note, if $u(i-1/2)<0$, one should use values at $i-1, i$, and $i+1$ to estimate ϕ at $i-1/2$. Estimation at $i+1/2$ can be made in the same way. The formula for estimating the value at $i-1/2$ with $u(i-1/2)>0$ is given in (Gaskell and Lau 1988):

$$\hat{\phi}_{i-1/2}=\begin{cases}\hat{\phi}_{i-1} & \text{if } \hat{\phi}_{i-1}\in[0,\ 1] \quad (1)\\ 3\hat{\phi}_{i-1} & \text{if } \hat{\phi}_{i-1}\in[0,\ 1/6] \quad (2)\\ \frac{3}{8}(2\hat{\phi}_{i-1}+1) & \text{if } \hat{\phi}_{i-1}\in[1/6,\ 5/6] \quad (3)\\ 1 & \text{if } \hat{\phi}_{i-1}\in[5/6,\ 1] \quad (4)\end{cases} \tag{17}$$

where $\hat{\phi}_{i-1/2}$, $\hat{\phi}_{i-1}$ are normalized values of $\phi_{i-1/2}$ and ϕ_{i-1}, respectively, defined as

$$\hat{\phi}_{i-1/2}=\frac{\phi_{i-1/2}-\phi_{i-2}}{\phi_i-\phi_{i-2}}, \tag{18}$$

$$\hat{\phi}_{i-1}=\frac{\phi_{i-1}-\phi_{i-2}}{\phi_i-\phi_{\cdot i-2}} \tag{19}$$

Eq. (17–1) is the backward differencing upwinding scheme for the non-monotonic variation of ϕ, Eq. (17–3) is the QUICK scheme for monotonic variation of ϕ, Eq. (17–2) and Eq. (17–4) are transition curves between Eq. (17–1) and Eq. (17–3). The main difference between Eq. (17) and ULTIMATE is Eq. (17–2) which may be outside the limiter when the Courant number is less than 1/6. To secure a unique solution in the region (5/6, 1], equation Eq. (17–4) was slightly modified as

$$\hat{\phi}_{i-1/2}=0.95+0.05\hat{\phi}_{i-1}. \tag{20}$$

It was found that the SMART scheme has problems to converge when it is used for solving non-linear Navier-Stokes equations for such a complicated flow field as the side discharge flow. Hence, some minor modifications of equations (17–2) and (20) were adopted. According to equations (18) and (19), equations (17–2) and (20) may be written in a dimensional form as (21) and (22), respectively:

$$\phi_{i-1/2}=3\phi_{i-1}-2\phi_{i-2}, \tag{21}$$

$$\phi_{i-1/2}=0.05\phi_{i-1}+0.95\phi_i. \tag{22}$$

If these expressions were used to solve a non-linear problem, they would probably cause instability as confirmed by the authors' numerical tests. To modify these equations, equations (18) and (19) were used, the final formulas being:

$$\phi_{i-1/2}=\phi_{i-1}-\frac{2\hat{\phi}_{i-1}}{1-\hat{\phi}_{i-1}}(\phi_{i-1}-\phi_i),\quad \hat{\phi}_{i-1}\in[0,1/6], \tag{23}$$

$$\phi_{i-1/2} = \phi_{i-1} + 0.95\left(\frac{1}{\hat{\phi}_{i-1}} - 1\right)(\phi_{i-1} - \phi_{i-2}), \quad \hat{\phi}_{i-1} \in (5/6, 1]. \tag{24}$$

After the above changes, (21) becomes equivalent to expression (23), and the equivalent expression for (22) is equation (24). Numerical tests for flow field simulation demonstrated that equations (23) and (24) converge while (21) and (22) do not.

Table 1. Comparison of computed recirculation length (L/h_0) for case 2. The measured length was $L/h_0 = 33$

	HYBRID	QUICK	SMART
Fine Grid, $L/h_0 =$	18	38	32
Coarse Grid, $L/h_0 =$	16	38	31

Table 2. Caluclated and measured [2] sizes of recirculation zones for smooth bed: $B = 1.82$ m, $h_0 = 0.06$ m, and rough bed: $B = 1.82$ m, $h_0 = 0.053$ m

Case	V_d (m/s)	U_0 (m/s)	b (m)	bed	H (m)	H (m) measured	L (m)	L (m) measured
1	0.03	0.1	0.3	smooth	0.11	0.13	1.92	1.86
2	0.4	0.1	0.0225	smooth	0.35	0.39	2.00	2.04
3	0.6	0.1	0.0225	smooth	0.5	—	2.45	—
4	0.2	0.1	0.0225	smooth	0.11	—	0.8	—
5	0.6	0.07	0.0225	smooth	0.68	—	2.9	—
6	0.6	0.06	0.0225	smooth	0.8	—	2.95	—
7	0.03	0.1	0.3	rough	0	0.1	0.053	0.69
8	0.4	0.1	0.0225	rough	0.18	0.19	1.1	1.2

To check the properties of the SMART scheme, the numerical simulations of the velocity field were made also by two other numerical schemes, HYBRID and QUICK (Table 1). These simulations were performed for Case 2 (see Table 2) and showed that the SMART converges slower than HYBRID, but faster than QUICK. Convergence of QUICK requires adjustment of a pseudo-transient coefficient (Han et al. 1981). If the solution of HYBRID was used as an illustrative solution, the SMART and QUICK scheme would converge much faster. Two mesh systems, $33 \times 22 \times 8$, and $45 \times 30 \times 8$ were generated to exam consistency, accuracy and numerical diffusion of these schemes. Mesh spacing near the bed, walls as well as near the discharge channel were made extra fine. The fine grid has almost twice as many nodes as the coarse one. Since the variation of the physical phenomena is much stronger in the horizontal than the vertical direction (water depth is small), the grid in the vertical was fixed. Table 1 summarizes the results of calculations by using the three different numerical schemes. The geometry of the simulated recirculation was obtained by measuring the shape of the computed trace lines.

These results indicate the accuracy of the SMART scheme. In fact, its result was closer to the data than the QUICK. Because solutions of SMART were not sensitive to the mesh size, the coarse mesh ($33 \times 22 \times 8$) was used for more simulations. These results confirmed the study of Demuren and Rodi (1983) that HYBRID scheme significantly underestimated the length of recirculation zone downstream the side discharge. This is due to the fact that the truncation error of the HYBRID scheme introduces the numerical diffusion that can be very large especially when the flow is skewed to the numerical grid. In this situation the numerical diffusion flux normal to a velocity vector occurs and leads to substantial errors. The numerical diffusivity in this direction can be expressed by formula [2]

$$\Gamma_n = \frac{uv(u^2 + v^2)\Delta x\,\Delta y}{2(u^3\Delta x + v^3\Delta y)} \tag{25}$$

where Δx, and Δy are grid sizes in the x and y directions, respectively. The ratio of the numerical to physical diffusivities was calculated for the HYBRID scheme, and is presented in Fig. 4. The maximum value of this ratio, in some areas, can be as high as 90, which is unacceptable.

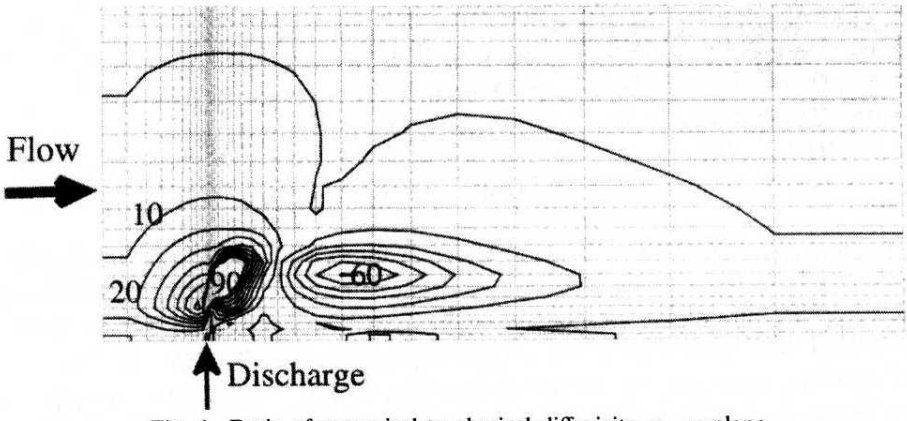

Fig. 4. Ratio of numerical to physical diffusivity, $x - y$ plane

The predicted reattachment distance with the QUICK scheme in this study, was greater than that of Demuren and Rodi [2], due, probably, to the differences in grid configurations and boundary conditions. As has been discussed, the current model prescribes k and ε at the inlet section with a different method. The inlet boundary conditions for the momentum equations were also different. The distance from the inlet section to the discharge channel was $4h_0$, and the primary velocity at this section in the transverse direction was constant in Demuren and Rodi's computation (1983). A much greater distance is equal to the $14h_0$ and 1/7 power law for transverse distribution of velocity were used in this study. Because

the case concerned subcritical flow, the side discharge would affect the upstream flow to some extent. It is reasonable to place the inlet section sufficiently far away from the side discharge to allow the flow to develop gradually upstream of the discharge channel. The maximum height of the recirculation zone for the simulated cases was about $13.3h_0$, $14h_0$ was thus adopted as the length of the approach channel for all simulation cases.

5. Computation Results and Discussion

The numerical simulations show that the vertical distributions of flow velocity direction and magnitude vary at different locations. The flow is three-dimensional especially along the trajectory of the side discharge, i.e., the velocity profiles are skewed, vectors near the bed are towards the recirculation zone and those near the water surface are towards to the main channel. The largest deviation appears in the immediate vicinity of the discharge channel, the deviation angles then decrease along the trajectory of the discharge. In the regions away from the trajectory, the flow turns gradually to two-dimensional in the vertical direction, i.e., the velocity vectors at one location from the bed to the surface are of the same direction. Fig. 5 shows the value of F computed using equation (26) and the flow condition of case 2 of Table 2.

$$F = |V_{surf}|\,|V_{bed}|\sin(V_{surf}, V_{bed}). \tag{26}$$

Where V_{surf} and V_{bed} are the velocity vectors taken very close to the water surface and to the channel bed, respectively. Higher values of F indicate greater magnitude of the vectors, as well as the deviation angle. The rapid decrease of F is mainly caused by the reduction of the angle, as the velocity reduces only gradually along the trajectory. One can note that the flow is strongly three-dimensional near the side discharge where strong mixing occurs.

The mathematical model described in previous sections has been verified as regards experimental measurements conducted by Rodi and Weiss (see Demuren and Rodi 1983) and Mihail et al. (1975). Rodi and Weiss made their experiments in both smooth and rough-bed channels with two different ratios of side discharge to cross-flow velocities, $R = 0.3$ and $R = 4$. The discharge channel width was $b = 0.3$ m for $R = 0.3$, and $b = 0.0225$ m was used for several cases with $R = 4$. Artificial roughness elements were applied to make the rough-bed channel. The pattern of recirculation was taken from photographs of the confetti particles sprayed onto the water surface. The values of the roughness parameter in the logarithmic law of the wall were chosen as $E = 9$ and $E = 0.065$ for the smooth and rough channel, respectively. In order to evaluate the capability of the model and to study the geometry of the recirculation zone in different flow conditions numerically, some more cases were simulated with flow conditions in the neighborhood of those used in the experiment. All of the simulated conditions are listed in Table 2.

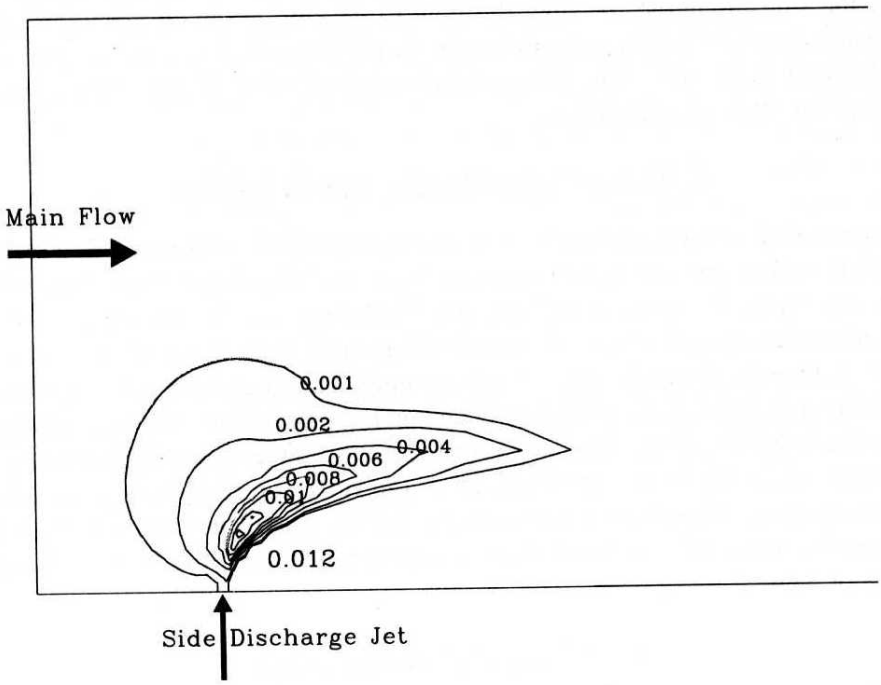

Fig. 5. Contour lines of F in the vicinity of a side discharge, $x - y$ plane (case 2, Table 2)

Fig. 6 shows the distribution of the longitudinal component of computed velocity at the water surface along the cross-section coming across the centre of the recirculation. To see the influence of the flow velocities of the main channel and that of the discharge, only those cases with smooth bed and the same width of the discharge channel (Cases 2, 3, 4, 5, and 6) were plotted. It is easy to note the influence of the side discharge on the lateral velocity distributions. When the discharge velocity is larger, the location of the maximum velocity is further from the discharge wall. The velocity near the opposite wall also increases in this case. The backward velocity in the recurculation zone responds similarly. In general, all the numerical simulations conform well with the data, with the exception of that for the rough bed channel at low side discharge (case 7), which does not show any recirculation whereas, the laboratory experiments shows some, although very small. The sizes of the recirculation zones for cases 1, 2, and 8 predicted by the model were the same as those measured. Although the recirculation in physical experiments showed multiple cells, all the simulated eddies had only a large single cell, the same as simulated by Demuren and Rodi (1983). One may need an extra

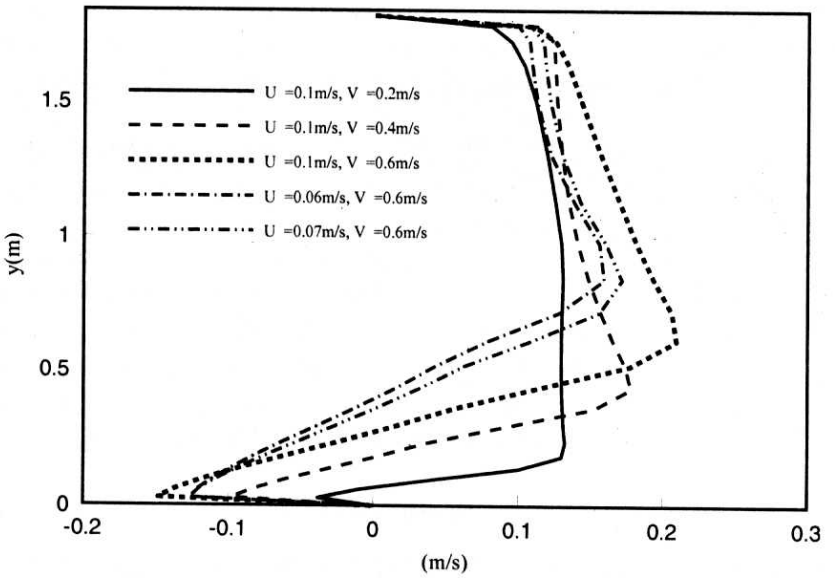

Fig. 6. Water surface velocity distribution across centre of recirculation zone, U = main channel velocity, V = discharge channel main velocity, y = distance from the discharge bank

fine grid and more complicated turbulence closure schemes to handle these small eddy structures.

Mikhail et al. (1975) carried out their measurements in a 61 cm wide open channel with a water depth of 5.1 cm. Side discharge velocities vary from 5 to 15 cm/s, and three widths of the discharge channel were used (0.64, 2.54, and 6.4 cm). Their dimensional analysis revealed that the non-dimensional size of the recirculation eddy (L/B and H/B) should be a function of the momentum flux ratio, R_m, only.

$$\frac{H}{B} = f_1(R_m), \quad \frac{L}{B} = f_2(R_m), \quad \text{where} \quad R_m = \frac{V_d^2 b}{U_o^2 B}. \tag{27}$$

In the case of very wide channels, the functions were supposed to be linear and the ratio H/L (eddy shape factor) should not depend on the momentum flux ratio.

The experimental data and the computational results (smooth bed) are plotted in Figures 7 and 8. It can be seen that the numerical model faithfully reproduce the characteristics of the recirculation eddy observed in physical modelling. Function f_1, initially (Fig. 7), grows with R_m almost linearly, and this slows down gradually at a higher value of R_m. There is one pair of data (measurement and calculation) representing the case with a very wide discharge channel, ten times wider than the remaining cases (case 1, Table 2). These data do not follow the main trend, which is characterized by narrow discharge channels. Mikhail et al. (1975) suggested that

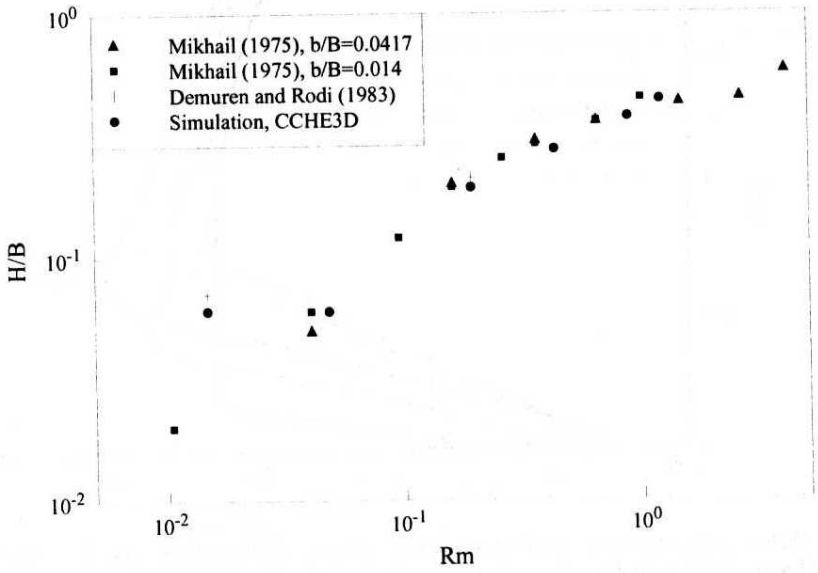

Fig. 7. Variation of recirculation zone height factor H/B with momentum flux ratio

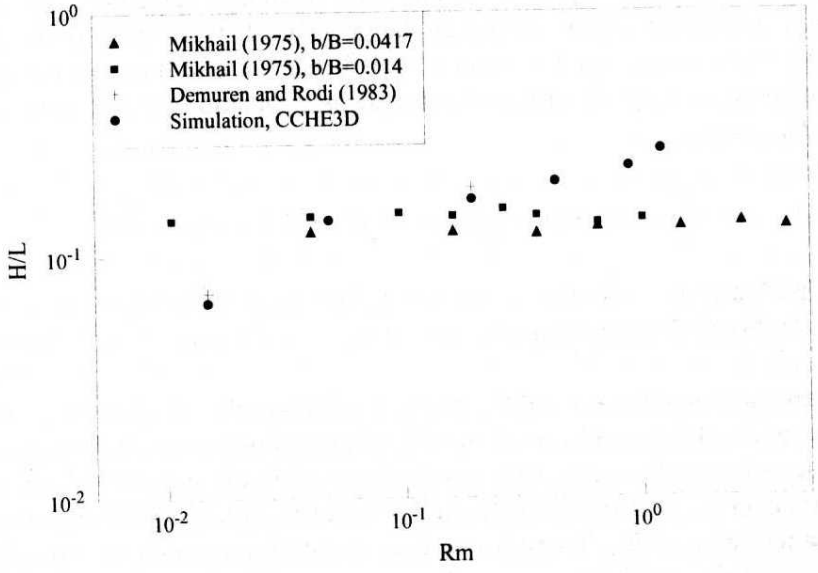

Fig. 8. Variation of recirculation zone shape factor as a function of momentum flux ratio

H/B approximately approaches a constant, 0.7. This is perhaps influenced by the opposite wall: having a larger recirculation height would have stronger constraint from the opposite wall. It can be seen that the wall constraint effect starts from about $R_m=0.2$.

The eddy shape factor indicates a slight divergence with the Mikhail data: H/L would remain a constant, equal to 0.13 for all the values of R_m (Fig. 8). The data from (Demuren and Rodi 1983) and the numerical simulation results show that this relationship is not universal: H/L increases with R_m when R_m is large. The shape factor might also be related to other hydraulic conditions in addition to R_m. It is not possible to simulate Mikhail's experiments since only some non-dimensional relationships are available. In order to fully verify the applicability of equation (27) to general practices, further research works are needed including both physical experiments and numerical simulations.

6. Conclusions

The mathematical model presented in the paper is capable of simulating a 3-D velocity field in the vicinity of a side discharge channel. The characteristic sizes of the recirculation zone (height and length) are estimated correctly in comparison with laboratory measurements. The simulations also show good conformity with the characteristic shape of the recirculation zone developed by Mikhail et al. (1975), differences might result from the experimental condition of the two sets of data. The mathematical model could not predict multi-cell structure in the recirculation eddy as observed in the experiments. Further research on better turbulence closure schemes has to be conducted where detailed flow structure within the recirculation is concerned.

The SMART scheme preserves the accuracy of the QUICK scheme, and reduces or eliminates its oscillation nature with high gradient of concentration, the SMART scheme is therefore more stable and converges faster than QUICK. The HYBRID scheme reveals strong numerical diffusivity, and predicts only about half the size of the recirculation zone with a fine grid. Minor modifications are necessary to improve the SMART capability in handling complex flow problems in transition regions. The "universal" relations (8, 9) for estimating the turbulence intensity can provide reliable boundary conditions for $k-\varepsilon$ model in calculating open channel flows.

Acknowledgment

This work is a result of research supported in part by the USDA Agriculture Research Service under Specific Research Agreement No. 5864087035 (monitored by the USDAARS National Sedimentation Laboratory and the University of Mississippi) and by the Polish Committee for Scientific Research under grant No. 6 P04D 020 20.

References

Demuren A. O. (1983), Numerical calculations of steady three-dimensional turbulent jet in cross flow, *Computer Methods in Applied Mechanics and Engineering*, 37, 309–328.

Demuren A. O., Rodi W. (1983), Side Discharge into Open Channels: Mathematical Model, *Journal of Hydraulic Engineering*, ASCE 109, 1707–1722.

Falconer R. A. (1992), Flow and Water Quality Modelling in Coastal and Inland Water, *Journal of Hydraulic Research*, 30, 437–452.

Gaskell P. H., Lau A. K. C. (1988), Curvature-Compensated Convective Transport: SMART, A New Boundedness-preserving Transport Algorithm, *International Journal for Numerical Methods in Fluids*, 8, 617–641.

Han T., Humphrey J. A. C., Launder B. E. (1981), A Comparison of Hybrid and Quadratic-upstream Differencing in High Reynolds Number Elliptic Flows, *Computer Methods in Applied Mechanics and Engineering*, 29, 81–95.

Jia Y., Wang S. Y. (1993), 3-D numerical simulation of flow near a spur dike. Proceedings, *Advances in Hydroscience and Engineering*, 1, part 2, 2150–2156.

Leonard B. P. (1979), A Stable and Accurate Convective Modelling Procedure Based on Quadratic Upstream Interpolation, *Computer Methods in Applied Mechanics and Engineering*, 19, 59–98.

Leonard B. P., Niknafs H. S. (1991), Sharp monotonic resolution of discontinuities without clipping of narrow extrema, *Computers & Fluids* , 19, 141–154.

Leschziner M. A. (1980), Practical evaluation of three finite difference schemes for the computation of steady-state recirculation flows, *Computer Methods in Applied Mechanics and Engineering*, 23, 293–312.

Long D., Steffler P. M., Rajaratnam N. (1991), A Numerical Study of Submerged Hydraulic Jumps, *Journal of Hydraulic Research*, 29, 293–308.

McGuirk J. J., Rodi W. (1978), A depth-averaged mathematical model for side discharges into open channel flow, *J. Fluid Mechanics*, 86, 761–781.

Mikhail R., Chu V.., Savage S. B. (1975), The reattachment of the two-dimensional turbulent jet in a confined cross flow, *Proceedings, 16th International Association for Hydraulic Research Congress*, Sao Paulo, Brazil, 3, 414–419.

Nezu I., Rodi W. (1986), Open-Channel Flow Measurements with a Laser Doppler Anemometer, *Journal of the Hydraulic Engineering*, ASC, 112, 335–355.

Patankar S. V. (1980), *Numerical Heat Transfer and Fluid Flow*, Taylor & Francis.

Rastogi A. K., Rodi W. (1980), Predictions of heat and mass transfer in open channel flow, *Journal of the Hydraulic Division*, ASCE, 104, 397–420.

Rodi W., Srivatsa S. K. (1980), A locally elliptic calculation procedure for three-dimensional flows and its application to a jet in a cross flow, *Computer Methods in Applied Mechanics and Engineering*, 23, 67–83.

Strazisar A., Prahl J. (1973), The effects of bottom friction on river entrance flow with crossflow, *Proceedings, 16th Conference Great Lakes Research*, 615–625.